PAPER

Check for updates

Schiff base derived Fe³⁺-selective fluorescence turn-off chemsensors based on triphenylamine and indole: synthesis, properties and application in living cells†

Chengqiang Pan,[a] Kai Wang,[a] Shaomin Ji,[a] Huaqian Wang,*[a] Zongzhi Li,[a] Huahong He[b] and Yanping Huo ⓘ *[ac]

Two Schiff base derivatives (S1 and S2) containing triphenylamine and indole fluorophores groups have been synthesized *via* a one-pot reaction and utilized as fluorescence turn-off sensors towards Fe³⁺ ions in THF. S1 and S2 demonstrated fluorescence turn-off sensing towards Fe³⁺ ions, *via* photoinduced electron transfer (PET). The 2 : 1 stoichiometries of the sensor complexes ([S1, S2] + Fe³⁺) were calculated from Job plots based on UV-vis absorption titrations. The detection limits (LODs) of [S1, S2] + Fe³⁺ sensor responses were calculated by their standard deviation, linear fitting and from their fluorescence binding isotherms. More importantly, [S1, S2] + Fe³⁺ sensors were found to be active in aqueous media within a wide range of pH values. In addition, biological imaging and membrane permeability demonstrated that S1 could act as a turn-off fluorescence chemosensor for Fe³⁺ in living cells.

1. Introduction

The design and synthesis of high selectivity and sensitivity chemical sensors to detect metal ions in the ecological environment and in biology has attracted a great deal of attention.[1–9] Current chemosensors present a large number of appealing advantages, including high sensitivity and selectivity, generally non-destructive characteristics, low cost, facile operation, a fast response time, and suitability as a diagnostic tool for biological purposes.[10–12]

As one of the essential trace elements in biological systems, Fe³⁺ plays a crucial role in living organisms and metabolism.[13,14] For example, it is an essential element for the formation of the hemoglobin of vertebrate red cells and plays an vital role in the storage and transport of oxygen to tissues.[15,16] However, iron level should be balanced in human being. Excessive Fe³⁺ in the human body has been found to be related to an increased incidence of certain cancers and the dysfunction of certain organs, with symptoms such as diarrhea, vomiting, stomach pain, and heart/liver damage.[17,18] On the other hand, iron deficiency can lead to anemia.[19] Hence a convenient and rapid

method for detecting the concentration of Fe³⁺ in biological samples is of great interest in biological and environmental concerns. Recently, some turn-off chemosensors for Fe(III)-selective detection were reported and a few of them have been successfully used in biological applications.[20] However, some defects of these chemosensors such as synthetic difficulties, ligand cytotoxicity, cross-sensitivity toward other metal cations, poor water solubility, a narrow pH detection span, a low fluorescence quantum yield in aqueous media, and long response times, have been found in actual practice.[21–28] Therefore, we tend to develop the specific sensory for Fe³⁺ detections in aqueous media with low cytotoxicity, a high fluorescence quantum yield and a broad pH detection span *via* simple synthetic pathways.

Currently, the fluorogenic materials with aggregation-induced emission (AIE) attributes have become a hot research topic since the debut of AIE concept in 2001,[29] and have been found to serve as chemosensors, bioprobes, stimuli-responsive nanomaterials and active layers in the construction of efficient organic light-emitting diodes.[30] However, many of these fluorogenic molecules also have synthetic difficulties, so we try to develop molecules that could exhibit the AIE effects with less synthetic difficulties.

With these considerations, Schiff bases are the suitable candidates having simple synthetic steps and also applied to many fluorescent sensors, as well as in AIE applications.[31,32] However, to develop Schiff base sensors with AIE properties, the presence of strong fluorophores are required.[33] Triphenylamine and indole derivatives were evidenced as excellent fluorophores and widely used in the developments of fluorescence (FL)

[a]School of Chemical Engineering and Light Industry, Guangdong University of Technology, Guangzhou 510006, China. E-mail: yphuo@gdut.edu.cn; huaqianwang@126.com; Fax: +86 20 39322235; Tel: +86 20 39322236; +86 13798135622; +86 13560355016

[b]Guangzhou Institute for Drug Control, Guangzhou 510160, China

[c]Guangdong Engineering Research Center for Scientific Research and Biochemical Detection Reagent, Guangzhou 510006, China

† Electronic supplementary information (ESI) available. See DOI: 10.1039/c7ra05064j
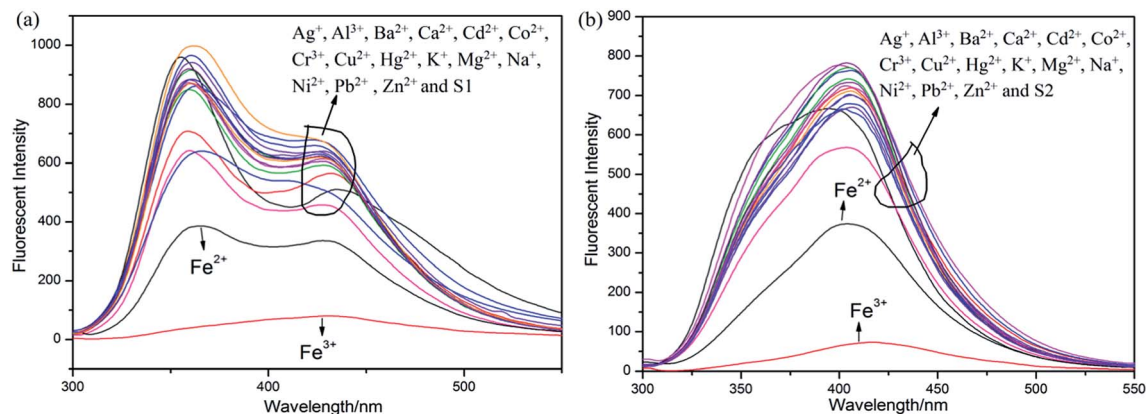
Fig. 1 Sensor responses of (a) **S1** and (b) **S2** (1×10^{-5} M) in THF (λ_{ex} = 300 nm) towards different nitrate salts in THF.

sensors because of their excellent photoluminescence properties and chemical stabilities. Therefore, we developed the triphenylamine- and indole- based Schiff bases and evaluated their sensor and AIE properties (Fig. 1).

Herein, we report triphenylamine- and indole- based Schiff bases derivatives (**S1** and **S2**) with AIE properties for the first time as Fe^{3+} turn-off sensors via PET and **S1** was also utilized for the detection of Fe^{3+} in living cells.
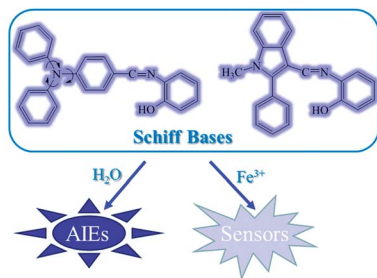
Schematic representations of sensors and aggregation induced emissions (AIEs) of Schiff bases.

2. Experimental

2.1 Materials and methods

All of the chemicals are commercially available, and used without further purification. Elemental analyses were performed with an EA1110 CHNS-0 CE elemental analyzer. All fluorescence measurements were carried out on a LS 50B Luminescence Spectrometer (Perkin Elmer, Inc., USA). All UV-vis absorption spectra were recorded on a Lambda 20 UV-vis Spectrometer (Perkin Elmer, Inc., USA). ^1H and ^{13}C NMR experiments were carried out on a MERCURYplus 400 spectrometer operating at a resonance frequency of 400 MHz. Electrospray ionization mass spectra (ESI-MS) were recorded on a Finnigan LCQ mass spectrometer. All the materials for synthesis were purchased from commercial suppliers and used without further purification. The metal ion solutions were prepared from $FeCl_2 \cdot 4H_2O$, $Ni(NO_3)_2 \cdot 6H_2O$, $Co(NO_3)_2 \cdot 6H_2O$, $Cu(NO_3)_2 \cdot 3H_2O$, $Mg(NO_3)_2 \cdot 6H_2O$, $Zn(NO_3)_2 \cdot 6H_2O$, $Ca(NO_3)_2 \cdot 4H_2O$, $Fe(NO_3)_3 \cdot 9H_2O$,

$Al(NO_3)_3 \cdot 9H_2O$, KNO_3, $NaNO_3$, $Cd(NO_3)_2 \cdot 4H_2O$, $Cr(NO_3)_3 \cdot 9H_2O$, $Hg(NO_3)_2 \cdot H_2O$, $Ba(NO_3)_2$ and $Pb(NO_3)_2$, respectively.

2.2 Synthesis of compound S1

2-Aminophenol (440.0 mg, 4.03 mmol) was added to a solution of 4-(diphenylamino)benzaldehyde (1096.05 mg, 4.01 mmol) dissolved in 30 ml of methanol. The resulting mixture was refluxed for 12 h. After completion of the reaction (confirmed by thin layer chromatographic analysis), the reaction mixture was filtered off and a light brown oily residue was obtained upon removal of the solvent from the filtrate under vacuum. This oily residue on treatment with ethanol gave an light brownish solid precipitate, which was collected by filtration and dried to give **S1** as a pure product (1095 mg, 75%). ^1H NMR (400 MHz, DMSO-d_6, TMS) δ (ppm): 9.52 (s, 1H), 8.26 (d, J = 8.6 Hz, 1H), 8.05 (d, J = 16.2 Hz, 1H), 7.75 (d, J = 8.6 Hz, 1H), 7.61 (d, J = 8.5 Hz, 2H), 7.34 (dd, J = 16.5, 9.3 Hz, 6H), 7.10 (t, J = 9.9 Hz, 6H), 7.00 (d, J = 8.5 Hz, 2H). ^{13}C NMR (500 MHz, $CDCl_3$, TMS) δ (ppm): 158.73, 151.52, 150.52, 146.93, 138.72, 130.69, 130.25, 127.31, 125.67, 124.72, 121.22, 119.93, 119.30, 116.24. ESI-MS m/z: 365.1 ($[M + H]^+$). Elemental analysis: found C: 82.12, H: 5.21, N: 7.28; calculated for ($C_{25}H_{20}N_2O$) C: 82.42, H: 5.49, N: 7.69 (%).

2.3 Synthesis of compound S2

2-Aminophenol (445.25 mg, 4.08 mmol) was added to a solution of 1-methyl-2-phenyl-3-formylindole (952.92 mg, 4.05 mmol) dissolved in 30 ml of methanol. The resulting mixture was
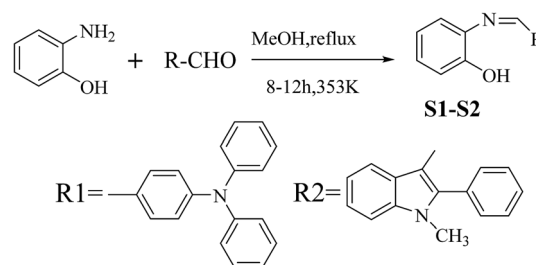
Scheme 1 Synthesis of **S1–S2**.

refluxed for 10 h. After completion of the reaction (confirmed by thin layer chromatographic analysis), the reaction mixture was filtered off and a light brown oily residue was obtained upon removal of the solvent from the filtrate under vacuum. This oily residue on treatment with ethanol gave an light brownish solid precipitate, which was collected by filtration and dried to give **S2** as a pure product (911.38 mg, 69%). ^1H NMR (400 MHz, DMSO-d_6, TMS) δ (ppm): 9.73 (s, 1H), 8.57 (s, 2H), 7.61–7.52 (m, 3H), 7.51–7.44 (m, 2H), 7.44–7.32 (m, 3H), 7.07 (t, $J = 7.2$ Hz, 1H), 6.99 (dd, $J = 11.2, 8.0$ Hz, 2H), 6.79 (t, $J = 7.6$ Hz, 1H), 3.66 (s, 3H). ^{13}C NMR (400 MHz, CDCl$_3$, TMS) δ (ppm): 152.75, 150.47, 146.54, 137.12, 136.83, 129.91, 128.71, 128.45, 127.68, 125.81, 124.41, 122.68, 121.41, 118.85, 114.42, 113.13, 112.08, 108.80, 30.05. ESI-MS m/z: 327.4 ([M + H]$^+$). Elemental analysis: found C: 80.54, H: 5.36, N: 8.28; calculated for (C$_{22}$H$_{18}$N$_2$O) C: 80.98, H: 5.52, N: 8.59 (%).

3. Results and discussion

3.1 Synthesis of S1–S2

As shown in Scheme 1, **S1** and **S2** were synthesized *via* a one pot aldehyde and amine condensation in methanol with 75 and 69% yields, respectively.

3.2 Spectroscopic properties

Initially, **S1** and **S2** (20 μM) in THF were investigated towards 60 μM (3 equiv.) of metal ions (Ag$^+$, Al^{3+}, Ba^{2+}, Ca^{2+}, Cd^{2+}, Co^{2+}, Cr^{3+}, Cu^{2+}, Fe^{2+}, Fe^{3+}, Hg^{2+}, K$^+$, Mg^{2+}, Na$^+$, Ni^{2+}, Pb^{2+} and Zn^{2+}) in H$_2$O. As noticed in Fig. 1, **S1** and **S2** show better selectivities to Fe^{3+} ions, respectively, upon treatment with 3 equiv. of metal ions, respectively. In addition, in order to establish the specific selectivities of **S1** and **S2** to Fe^{3+}, respectively, we performed the single and dual metal competitive analysis, as shown in Fig. 2. In a single metal system (black bars), all the metal (Ag$^+$, Al^{3+}, Ba^{2+}, Ca^{2+}, Cd^{2+}, Co^{2+}, Cr^{3+}, Cu^{2+}, Fe^{2+}, Fe^{3+}, Hg^{2+}, K$^+$, Mg^{2+}, Na$^+$, Ni^{2+}, Pb^{2+} and Zn^{2+} in H$_2$O) concentrations were kept as 60 μM. However, for the dual-metal (red bars) studies, two equal amounts of aqueous solutions of Fe^{3+} and other metal ions (60 μM + 60 μM) were combined. Furthermore, in the single metal analysis, the Fe^{3+} effect at 60 μM was investigated. In addition to the selectivity of **S1** and **S2** towards Fe^{3+} ion, Fe^{2+} ion also showed little selectivity (Fig. 1).

Moreover, the specific selectivities of **S1** and **S2** by single and dual metal studies also conformed their respective selectivities toward Fe^{3+} ion. The effect of Fe^{3+} concentration on the
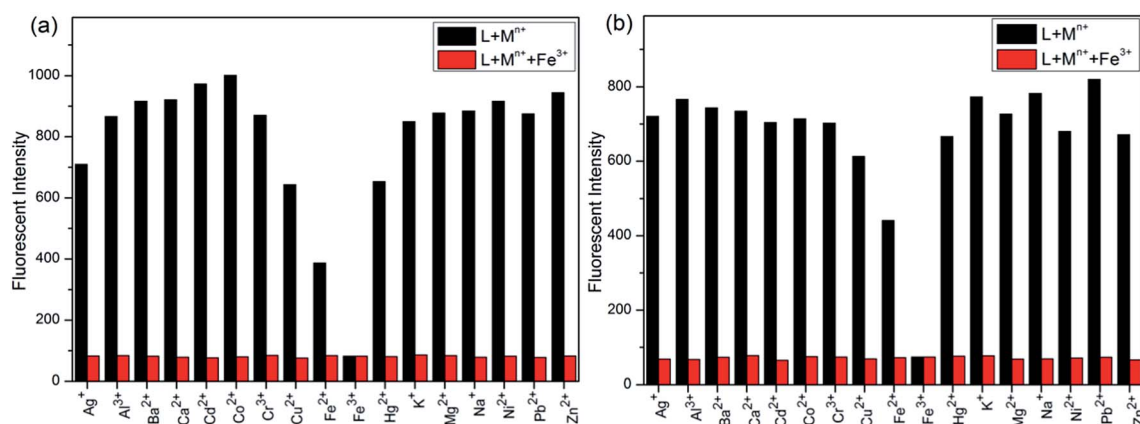

Fig. 2 Relative fluorescence intensities of (a) **S1** and (b) **S2** in THF ($\lambda_{ex} = 300$ nm) in THF in the presence of competing metal ions. Black bar; **S1** and **S2** in THF with stated metal ions in H$_2$O, respectively. Red bar; **S1** and **S2** in THF with Fe^{3+} + stated metal ions in H$_2$O.
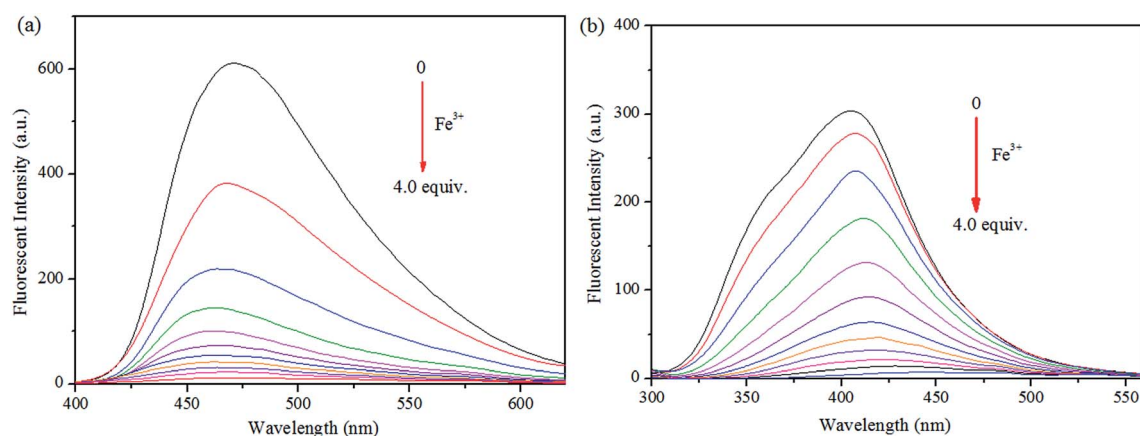

Fig. 3 Fluorescence spectra of (a) **S1** and (b) **S2** and in THF ($\lambda_{ex} = 300$ nm) with 0–4 equiv. of Fe^{3+} in H$_2$O.
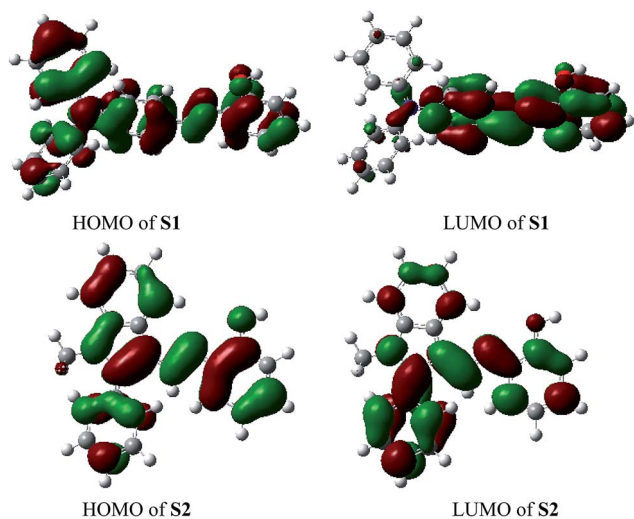
HOMO of **S1**   LUMO of **S1**

HOMO of **S2**   LUMO of **S2**

Fig. 4 Molecular orbitals of HOMO and LUMO for **S1–S2**.

Monomer-Blue Emission   Excimer-Weak Emission

Fig. 6 Possible proposed binding mechanism of **S1** or **S2**, towards Fe^{3+} ions.

emission of **S1** and **S2** was investigated in detail. Fig. 3 illustrates the fluorescence spectral changes of **S1** and **S2** (20 μM) as a function of Fe^{3+} concentration (0–4.0 equiv.) in THF at room temperature. Importantly, as the concentration of the Fe^{3+} ions increased, a progressive decrease in the fluorescence emission intensity at 470 nm and 405 nm was observed, respectively.

For better understanding of the chromofluorophore, DFT study was done for **S1** and **S2**. All theoretical calculations were carried out using the Gaussian 09 program. The B3LYP exchange correlation functional under LANL2DZ basis set was performed to calculate HOMO and LUMO levels. The geometries were optimized, and electron distribution in the MOs was calculated (Fig. 4). The HOMO–LUMO orbital distribution showed that the electron cloud of **S1** was spread from the phenylamine moiety to the phenol moiety. The major contribution for HOMO and LUMO of **S2** was well-distributed. Indeed, it has been demonstrated that fluorescence quenching of these compounds may occur by the photoinduced electron transfer (PET) from intraligand charge transfer.
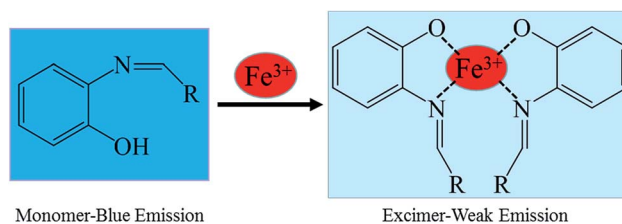
To ensure the binding sites of sensor responses of, the stoichiometries of **S1** or **S2** + Fe^{3+} were calculated through Job's plots as shown in Fig. 5. The stoichiometries of **S1** or **S2** + Fe^{3+} were established by Job's plots between the mole fraction (X_M) and absorption maximum changes at 435 nm, respectively. Upon the addition of 0–60 μM of Fe^{3+} (with an equal span of 6 μM). The Job's plots were plotted between X_M and absorption changes at 435 nm, where they went through maxima at molar fractions of *ca.* 0.323 and 0.385, respectively, as shown in Fig. 5, representing their 2 : 1 stoichiometric. From the ESI, the ESI mass spectrum of **S1** or **S2** and Fe^{3+} was also studied to find further support for this binding behavior. The complexes of **S1** or **S2** and Fe^{3+} show the peak at *m/z* 782 and 706, (calculated *m/z* 782 and 706 for **S1** or **S2** and Fe^{3+}), respectively, illustrating the structure of the complexes of **S1** or **S2** and Fe^{3+}, confirming the 2 : 1 stoichiometric ratio between the host and guest. Therefore, the possible sensing mechanism based on the excimer formation was proposed as noted in Fig. 6. The fluorescence changes observed in the ligand solutions of **S1** and **S2** upon binding to Fe^{3+} are due to deprotonation of phenolic –OH which allows the charge transfer from ligand to metal ion. The charge transfer from ligand to metal is also responsible for fluorescence quenching behavior of ligands upon metal complexation.[33]

In order to prove the selectivities of **S1** and **S2** towards Fe^{3+}, respectively, the calculations of detection limits (LODs) were performed through standard deviations and linear fittings as shown in Fig. 7. By plotting the relative fluorescence intensity (I_0/I) changes as a function of concentration the detection limits of **S1**
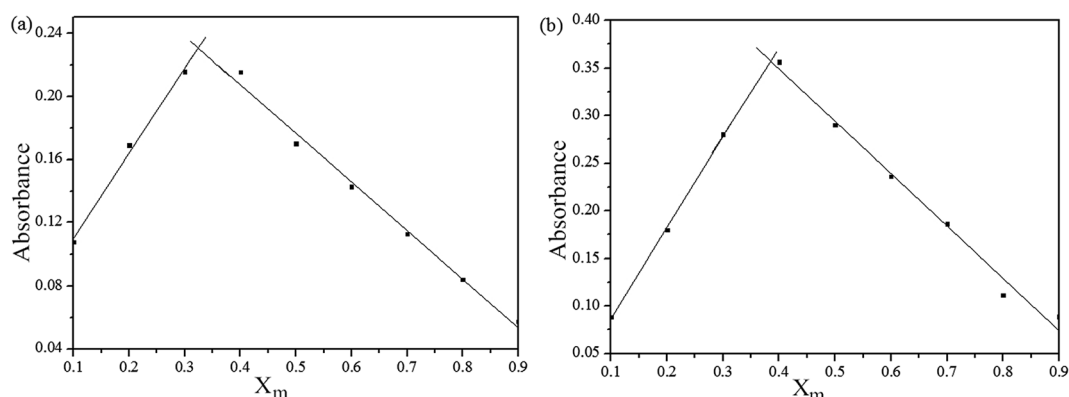

Fig. 5 Absorbance spectral changes of (a) **S1** and (b) **S2** in THF, titrated with of Fe^{3+} ions in H_2O and (b) stoichiometry calculations of (a) **S1** and (b) **S2** based on absorbance changes; $X_m = [Fe^{3+}]/[Fe^{3+}] + [S]$; where X_m = mole fraction, $[Fe^{3+}]$ and [S] are concentrations of Fe^{3+} and **S1** or **S2**.
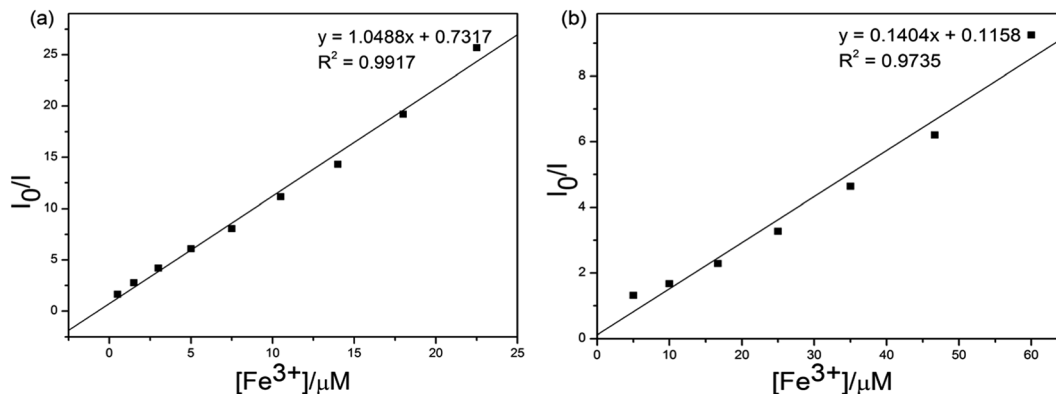
Fig. 7 Standard deviations and linear fitting for detection limit calculations of (a) **S1** and (b) **S2** + Fe^{3+}.

or **S2** + Fe^{3+} were calculated as 4.51×10^{-5} and 3.37×10^{-6} M, respectively. The detection limit (LODs) was determined from the following equation: LODs = $3\sigma/S$ where σ is the standard deviation of the blank solution; S is the slope of the calibration curve.

Considering the influence of pH to the sensors. The **S1** or **S2** and **S1** or **S2** + Fe^{3+} sensors responses were verified between pHs 0 and 14, maintained by the respective buffers (100 μM). In contrast to separate titrations of pHs (0–14) solutions (100 μM) to **S1** and **S2**. The experiment results show that the sensors of **S1** or **S2** were stable in wide ranges of pHs 3–12 and 4–12, respectively (see Fig. 8). Meanwhile the **S1** or **S2** + Fe^{3+} sensors were active in wide ranges of pHs 1–14 in both cases, as shown in Fig. 8. The experiment results show that **S1** or **S2** + Fe^{3+} were stable in wide ranges of pHs 3–12 and 4–12 respectively. In pH 3–12, due to ESIPT involving the phenolic protons and C=N isomerization. The C=N isomerization is the predominant decay process of the excited state for **S1** and **S2**. Upon addition of Fe^{3+}, the coordination of **S1** and **S2** with the metal ion inhibits the C=N isomerization and prevents ESIPT.[34] But fluorescence dramatically change from pH 12 are most likely caused by the deprotonation of the hydroxy group of **S1** and **S2**.[35] The above observation confirmed that the sensors can be utilized in acidic and basic and not affected by pH change.

Since many sensor responses are affected by the presence of counter ions, we performed the sensor titrations of **S1** and **S2** towards Fe^{3+}, respectively, with different counterion salts. As evidenced in Fig. 9, the Fe^{3+} sensor response was found to be decreased in the presence of counter ions (Br^-, NO_3^-, Cl^-, F^-, ClO_4^-, OH^- and SO_4^{2-}). Hence, it was concluded that both the Fe^{3+} sensor responses of **S1** and **S2** were not affected incredibly in the presence of different counter ions.

More interestingly, while preparing the stock solutions of **S1** and **S2** in THF by varying the water concentrations for sensor titrations, the fluorescence spectra were enhanced with spectral shifts due to their aggregated nature. Hence, we proceeded the aggregation induced enhanced emission (AIEE) analysis further. As shown in Fig. 10, the PL intensities were enhanced by increasing the concentrations of H_2O (up to 90% or 80%), at the same time, the PL emissions were shifted from 460 to 479 nm of **S1** and 430 to 424 nm of **S2** in both extremes. The fluorescence changes arose from AIE were visualized by the photographs of **S1** (0 and 80%) and **S2** (0 and 90%), respectively.

As reported by previous literature,[36] the AIEs mechanism of both **S1** and **S2** possibly arose from the restriction of intramolecular rotation (RIR). Since, the single bond rotation is mainly responsible for the dominant nonradiative decay. A
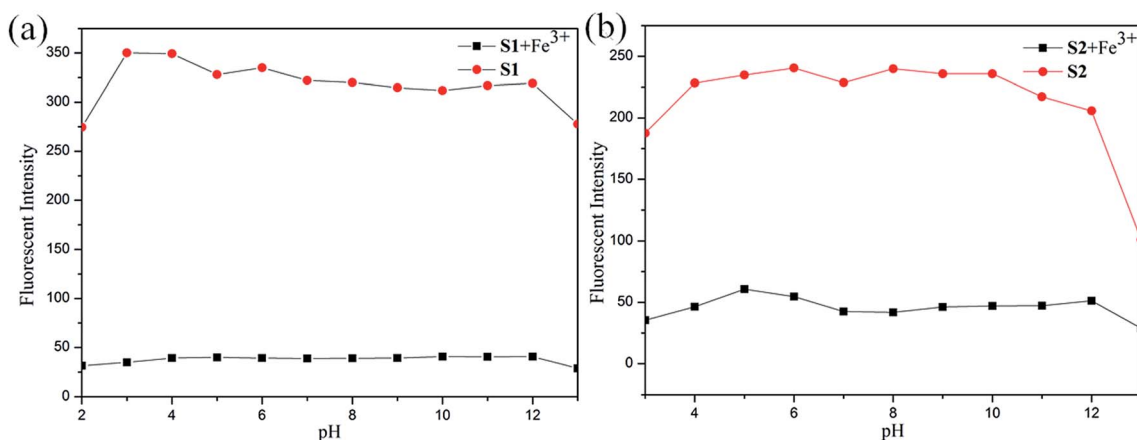

Fig. 8 Fluorescence intensity of (a) **S1** and (b) **S2** with different pH conditions.
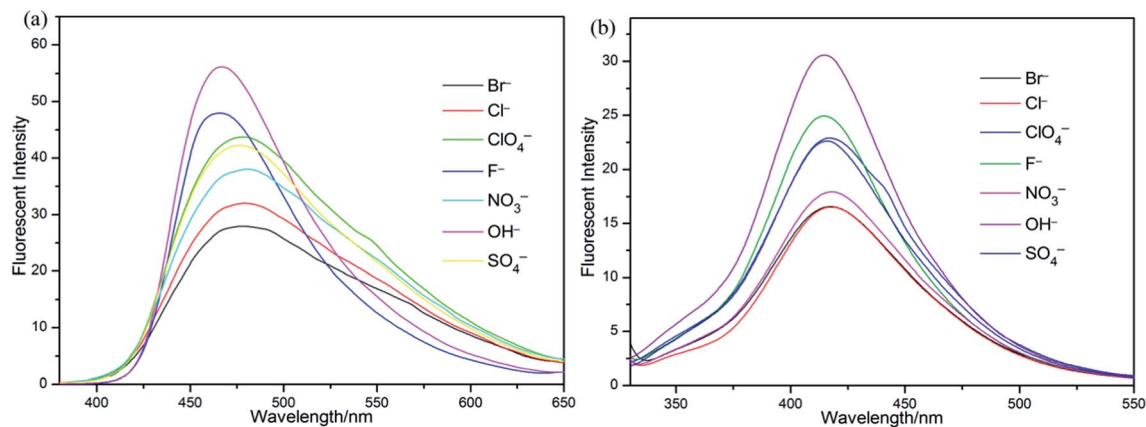
Fig. 9 Sensor responses of (a) **S1** and (b) **S2** towards Fe^{3+} in presence of different counter ions.
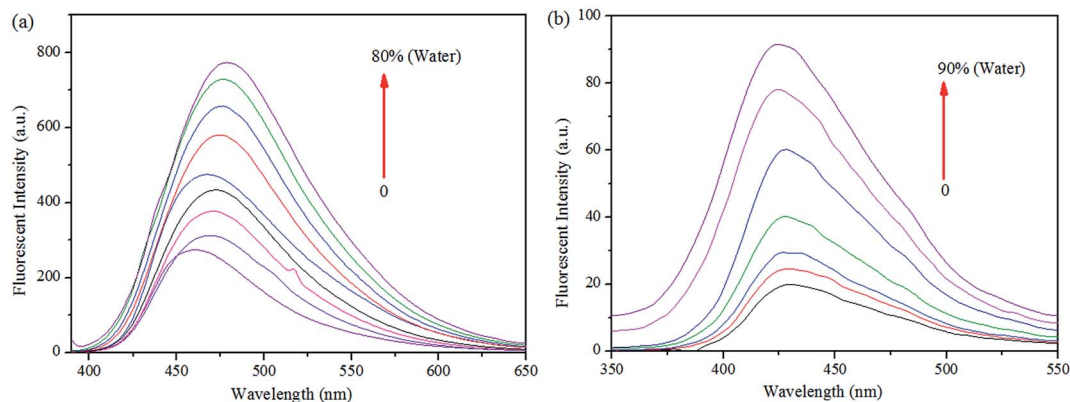

Fig. 10 Fluorescence spectra of (a) **S1** and (b) **S2** in THF, upon increasing the concentration of water.

single bond that links a benzene ring of **S1** and **S2** can be rotated. The RIR effect might be the cause for the AIEE nature of **S1** and **S2**. The PET process and suppression of charge transfer (CT) or intramolecular charge transfer (ICT) are the other mechanistic approaches for AIE. However, our observations on the PL spectra of AIEEs for **S1** and **S2** suggested that both the red and blue shifts by aggregation were probably originated from the suppression of twisted intramolecular charge transfer (TICT). The above justification was also well

supported by the similar reports available in the field of AIEs.[37]

To demonstrate the potential of **S1** to detect Fe^{3+} in living matrices, fluorescence imaging experiments were carried out in living cells (Fig. 11). First, we selected human prostatic carcinoma cell line (PC-3) to investigate the permeability of **S1**. PC-3 cells were obtained from the Cell Resources Center of the Shanghai Institutes for Biological Sciences, Chinese Academy of Sciences. Human prostate cancer cell PC-3 was derived from
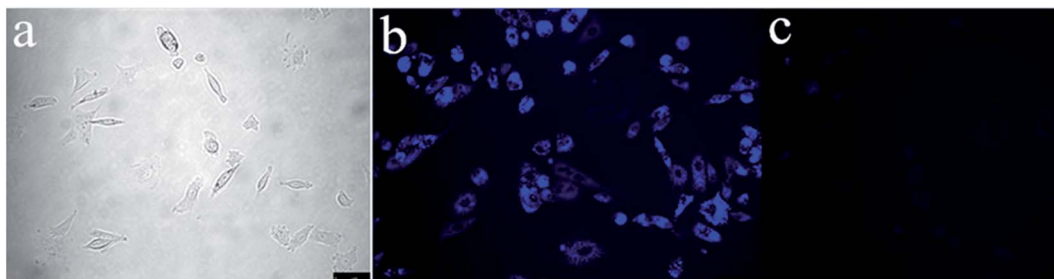

Fig. 11 Fluorescence microscopy images of Fe^{3+} in PC-3 cells (Olympus IX71, 40× objective lens). (a) Bright-field transmission image of PC-3 cells. (b) Fluorescence image of PC-3 cells incubated with **S1** (10 μM). (c) Further incubated with addition of various concentrations of Fe^{3+} (10 equiv.).

a 62 year-old grade IV prostate cancer in white male patients with bone marrow metastases. The patient with prostate cancer signed informed consent before any study procedures. The cells were cultured in RPMI 1640 (Gibco) and supplemented with 10% fetal bovine serum (FBS; Gibco) at 37 °C in a humidified atmosphere of 5% CO_2. For all experiments, cells were harvested from subconfluent cultures by the use of trypsin and were resuspended in fresh complete medium before plating. PC-3 cells were incubated with S1 (10 μM) for 1 h at 37 °C, and washed with PBS to remove the remaining compound S1. The results are shown in Fig. 11. One can clearly observe significant imaging changes of the medium upon addition of Fe^{3+} for 30 min (10 equiv.) at 37 °C. PC-3 cells incubated with S1 initially display a strong fluorescence image (Fig. 11b), but the fluorescence image immediately becomes faint even quenching in the presence of Fe^{3+} (Fig. 11c). Thus, the chemosensor S1 can be a suitable fluorescence chemosensing probe for Fe^{3+} detection in biological systems.

At the same time, we also studied the fluorescence imaging of S2 in PC-3 cells. But the results showed that PC-3 cells incubated with S2 initially almost no fluorescence angiography (Fig. S2†), which suggests that the AIE phenomenon of S2 was unobvious compared with the S1. In the medium solution, both S1 and S2 have an AIE effect. As shown in Fig. 10, the AIE phenomenon of S1 was significantly better than S2. The fluorescence intensity of S2 was weak in the medium solution. So there was no fluorescence of S2 in PC-3 cells.

4. Conclusion

In summary, two Schiff based turn-off chemosensors with AIE were designed for detection of Fe^{3+}, which were investigated with much higher selectivity over other competitive metal ions. Adequate characterization and studies were carried out to confirm the chemosensors S1 and S2 and their sensing behaviors toward Fe^{3+} ion. The 2 : 1 stoichiometry of sensors to Fe^{3+} were calculated from Job plots based on UV-vis absorption titrations. Furthermore, by standard deviations and linear fittings the detection limits (LODs) of S1 or S2 + Fe^{3+} were calculated as 4.51×10^{-5} and 3.37×10^{-6}, respectively. And their recognition behavior can function well over a wide range of pH, and not affected incredibly in the presence of different counter ions, making them suitable for detection of Fe^{3+} ion in industrial and environmental fields. As well as, fluorescence imaging experiments of S1 in living cells clearly observe good cell permeability and significant imaging changes of the aqueous solution medium upon addition of Fe^{3+}. Therefore, the turn-off chemosensor S1 can be a suitable fluorescence chemosensing probe for Fe^{3+} detection in biological systems. This is of great significance for medical research. Similar to the sensor properties, S1 and S2 in THF showed greater AIEE properties with shifted PL emission peaks.

Acknowledgements

References

1 E. M. Nolan and S. J. Lippard, *Chem. Rev.*, 2008, **108**, 3443–3480.

2 J. S. Kim and D. T. Quang, *Chem. Rev.*, 2007, **107**, 3780–3799.

3 S. K. Kim, D. H. Lee, J. I. Hong and J. Y. Yoon, *Acc. Chem. Res.*, 2009, **42**, 23–31.

4 E. M. Nolan and S. J. Lippard, *Acc. Chem. Res.*, 2009, **42**, 193–203.

5 R. Martínez-Mánez and F. Sancenón, *Chem. Rev.*, 2003, **103**, 4419–4476.

6 D. T. McQuade, A. E. Pullen and T. M. Swager, *Chem. Rev.*, 2000, **100**, 2537–2574.

7 C. R. Lohani and K. H. Lee, *Sens. Actuators, B*, 2010, **143**, 649–654.

8 H. N. Kim, M. H. Lee, H. J. Kim, J. S. Kim and J. Yoon, *Chem. Soc. Rev.*, 2008, **37**, 1465–1472.

9 M. Formica, V. Fusi, L. Giorgi and M. Micheloni, *Coord. Chem. Rev.*, 2012, **256**, 170–192.

10 A. T. Wright and E. V. Anslyn, *Chem. Soc. Rev.*, 2006, **35**, 14–28.

11 J. Liu and Y. Lu, *J. Fluoresc.*, 2004, **14**, 343–354.

12 J. H. Lee, Z. Wang, J. Liu and Y. Lu, *J. Am. Chem. Soc.*, 2008, **130**, 14217–14226.

13 O. K. Fix and K. V. Kowdley, *Minerva Med.*, 2008, **99**, 605–617.

14 P. Aisen, M. Wessling-Resnick and E. A. Leibold, *Curr. Opin. Chem. Biol.*, 1999, **3**, 200–206.

15 X. B. Zhang, G. Cheng, W. J. Zhang, G. L. Shen and R. Q. Yu, *Talanta*, 2007, **71**, 171–177.

16 K. Vijay, C. Nandib and S. D. Samant, *RSC Adv.*, 2016, **6**, 49724–49727.

17 (*a*) E. D. Weinberg, *Eur. J. Cancer Prev.*, 1996, **5**, 19–36; (*b*) D. Galaris, V. Skiada and A. Barbouti, *Cancer Lett.*, 2008, **266**, 21–29.

18 F. O. Omara and B. R. Blakley, *J. Nutr.*, 1993, **123**, 1649–1655.

19 L. H. Allen, *J. Nutr.*, 2002, **132**, 813S–819S.

20 (*a*) L. Huang, F. P. Hou, J. Cheng, P. X. Xi, F. J. Chen, D. Bai and Z. Z. Zeng, *Org. Biomol. Chem.*, 2012, **10**, 9634–9638; (*b*) S. K. Sahoo, D. Sharma, R. K. Bera, G. Crisponi and J. F. Callan, *Chem. Soc. Rev.*, 2012, **41**, 7195–7227; (*c*) B. K. Kanungo, M. Baral, R. K. Bera and S. K. Sahoo, *Monatsh. Chem.*, 2010, **141**, 157–168.

21 H. S. Jung, P. S. Kwon, J. W. Lee, J. I. Kim, C. S. Hong, J. W. Kim, S. H. Yan, J. Y. Lee, J. H. Lee, T. H. Joo and J. S. Kim, *J. Am. Chem. Soc.*, 2009, **131**, 2008–2012.

22 D. En, Y. Guo, B. Chen, B. Dong and M. Peng, *RSC Adv.*, 2013, **4**, 248–253.

23 K. Mehdi, B. Alireza and M. Ghodsi, *J. Fluoresc.*, 2015, **25**, 1297–1302.

24 R. Kagit, M. Yildirim, O. Ozay, S. Yesilot and H. Ozay, *Inorg. Chem.*, 2014, **53**, 2144–2151.

25 M. Kumar, R. Kumar, V. Bhalla, P. R. Sharma and T. Kaur, *Dalton Trans.*, 2012, **41**, 408–412.

26 L. Fu, J. Mei, J. Zhang, Y. Liu and F. Jiang, *Luminescence*, 2013, **28**, 602–606.

27 X. Zhang, G. Cheng, W. Zhang, G. Shen and R. Yu, *Talanta*, 2007, **71**, 171–177.

28 J. Nandre, S. Patil, P. Patil, S. Sahoo and C. Redshaw, *J. Fluoresc.*, 2014, **24**, 1563–1570.

29 Y. Hong, J. W. Y. Lam and B. Z. Tang, *Chem. Soc. Rev.*, 2011, **40**, 5361–5388.

30 (*a*) M. Wang, G. Zhang, D. Zhang, D. Zhu and B. Z. Tang, *J. Mater. Chem.*, 2010, **20**, 1858–1867; (*b*) Z. Liu, W. Xue, Z. Cai, G. Zhang and D. Zhang, *J. Mater. Chem.*, 2011, **21**, 14487–14491.

31 (*a*) V. Bhalla, R. Tejpal, R. Kumar and A. Sethi, *Inorg. Chem.*, 2009, **48**, 11677–11684; (*b*) D. Maity, A. K. Manna, D. Karthigeyan, T. K. Kundu, S. K. Pati and T. Govindaraju, *Chem.–Eur. J.*, 2011, **17**, 11152–11161; (*c*) S. Sumalekshmy and C. J. Fahrni, *Chem. Mater.*, 2011, **23**, 483–500; (*d*) D. Maity and T. Govindaraju, *Inorg. Chem.*, 2011, **50**, 11282–11284; (*e*) J. F. Jang, Y. Zhou, J. Yoon and J. S. Kim, *Chem. Soc. Rev.*, 2011, **40**, 3416–3429; (*f*) P. Song, X. Chen, Y. Xiang, L. Huang, Z. Zhou, R. Wei and A. Tong, *J. Mater. Chem.*, 2011, **21**, 13470–13475.

32 M. Shellaiah, Y. H. Wu, A. Singh, M. V. R. Raju and H. C. Lin, *J. Mater. Chem. A*, 2013, **1**, 1310–1318.

33 N. Narayanaswamy and T. Govindaraju, *Sens. Actuators, B*, 2012, **161**, 304–310.

34 L. Yang, W. Zhu, M. Fang, Q. Zhang and C. Li, *Spectrochim. Acta, Part A*, 2013, **109**, 186–192.

35 M. J. C. Marenco, C. Fowley, B. W. Hyland, G. R. Hamilton, D. Galindo-Riaño and J. F. Callan, *Tetrahedron Lett.*, 2012, **53**, 670–673.

36 (*a*) S. Karupannan and J. C. Chambron, *Chem.–Asian J.*, 2011, **6**, 964–984; (*b*) L. Fabbrizzi, M. Lichelli, P. Pallavicini, D. Sacci and E. Taglietti, *Analyst*, 1996, **121**, 1763–1768.

37 (*a*) M. Cai, Z. Gao, X. Zhou, X. Wang, S. Chen, Y. Zhao, Y. Qian, N. Shi, B. Mi, L. Xie and W. Huang, *Phys. Chem. Chem. Phys.*, 2012, **14**, 5289–5296; (*b*) Y. Hong, L. Meng, S. Chen, C. W. T. Leung, L. T. Da, M. Faisal, D. A. Silva, J. Liu, J. Wing, Y. Lam, X. Huang and B. Z. Tang, *J. Am. Chem. Soc.*, 2012, **134**, 1680–1689; (*c*) A. Qina, J. W. Y. Lamb and B. Z. Tang, *Prog. Polym. Sci.*, 2012, **37**, 182–209.